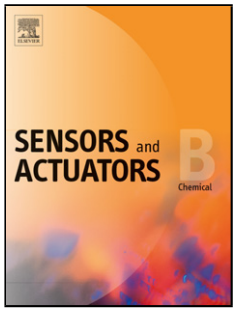


Title: Iridium and Ruthenium oxide miniature pH sensors: long-term performance

Authors: R.H.G. Mingels, S. Kalsi, Y. Cheong, H. Morgan

PII: S0925-4005(19)30979-7
DOI: https://doi.org/10.1016/j.snb.2019.126779
Article Number: 126779

Reference: SNB 126779

To appear in: *Sensors and Actuators B*

Received date: 17 April 2019
Revised date: 25 June 2019
Accepted date: 4 July 2019

Please cite this article as: Mingels RHG, Kalsi S, Cheong Y, Morgan H, Iridium and Ruthenium oxide miniature pH sensors: long-term performance, *Sensors and amp; Actuators: B. Chemical* (2019), https://doi.org/10.1016/j.snb.2019.126779

# Iridium and Ruthenium oxide miniature pH sensors: long-term performance

**R.H.G. Mingels[a,*], S. Kalsi[a], Y. Cheong[b], H. Morgan[a]**

[a] Electronics and computer Science, University of Southampton, Southampton, SO17 1BJ, UK

[b] School of Medicine, University of Southampton, Southampton, SO17 1BJ, UK

[*]Corresponding author. R.H.G.Mingels@soton.ac.uk

Research Highlights

- Iridium oxide Films and Ruthenium oxide films have excellent short-term pH sensing characteristics.
- Annealing of the RUOF increases the long-term stability of the film.
- Ruthenium oxide can be used in EIS at a reduced cost compared to Iridium oxide.
- Long-term pH sensing performance of EIROF is better compared to RUOF when the drift is characterised.
- RUOF does not suffer from a distinct drift and has consistent long-term performance over 4 weeks.

**Abstract**

The characteristics of electrodeposited Iridium oxide films (EIROF), and Ruthenium oxide films (RUOF) under normal and annealed conditions have been investigated. RUOFs were sputter deposited onto a substrate whilst EIROF sensors were made by electrodeposition. The adhesion of the RUOF sensors was investigated on Platinum and Titanium surfaces. The electrical impedance of the two metal oxides was measured in PBS demonstrating that both films have up to a 100 fold higher electrical double layer capacitance than bright Platinum electrodes. The EIROF films show super-Nernstian response, but the formal potential shows a continuous drift with time of approximately 2 mV $day^{-1}$, measured over 40 days. Both RUOF sensors show approximately Nernstian behaviour. Short term pH precision of the annealed RUOF falls within a confidence interval of ± 0.1 pH, and stability is maintained within a confidence of ± 0.24 pH for up to 147 days. The un-annealed RUOF

maintains the same precision but only for 20 days. Compared to EIROF sensors, no drift correction is required for the annealed RUOF making this metal oxide suitable for long term measurements where re-calibration is not possible.

**Key words:** Ruthenium oxide, Iridium oxide, pH Sensor, Impedance, long term sensing, metal oxide pH sensor.

## Introduction

There is a requirement for miniature, accurate and unobtrusive measurement of pH in many applications. The original glass pH probe was developed by *Haber* and *Klemensiewicz* in 1909, and its reliability, accuracy and life-time has made it one of the greatest sensors ever developed. Since then there has been a desire to mimic its performance on a miniature scale (1, 2). The advent of microfabrication tools in the early 1960s led to the development of ion sensitive field effect transistors and metal oxide (MO) based pH sensors (3-5). The ability to manufacture these solid-state sensors in a small footprint make these an attractive alternative to the glass pH sensor. Unfortunately, the reliability of these devices, and in particular their long-term performance, remains a major concern. Although regular re-calibration can be done, certain long-term applications, including *in vivo* sensing, remote environmental or maritime applications demand long term stability for periods exceeding 7 days, using the initial calibration. MO based devices are particularly attractive due to their much lower cost and potentiometric read-out capability, which reduces power requirements.

Iridium oxide ($IrO_x$) thin films have been widely used for pH measurement due to ease of deposition, wide linear range and biocompatibility (6-8). However, the performance and characteristics of $IrO_x$ can vary greatly, particularly long term. Furthermore, $IrO_x$ is one of the more expensive platinum group metals (9). Although it shows superior sensitivity, in many cases super-Nernstian with sensitivities above -60 mV $pH^{-1}$ due to its increased proton exchange capacity in the hydrated oxide film, application for long time monitoring is limited primarily due to long hydration times and delamination, limiting life-time to 2 months (6, 10-13). Thermally deposited films have longer lifetime but at the cost of reduced sensitivity. Unfortunately these are difficult to fabricate due to the high temperature required for oxide formation (12, 14-16). Lesser known metal oxides such as Ruthenium oxide ($RuO_x$) have similar sensitivity but are much less expensive. $RuO_x$ has been used for a variety of applications including in the biomedical field (17-20), however, a full characterisation has not been presented.

This paper characterises both the short and long-term (40 days) performance of Iridium and Ruthenium oxide pH sensors with respect to their key performance characteristics: sensitivity,

precision and drift. $IrO_x$ was made by electrochemical deposition, while $RuO_x$ was fabricated by sputtering. The ultimate goal is to develop a pH sensitive electrode with extended lifetime for *in vivo* applications, where recalibration cannot be performed. To mimic this, the characteristics of the final $RuO_x$ sensors were measured for 147 days during continuous immersion in phosphate buffered saline (PBS).

**Sensing mechanism.** The pH response of a metal oxide film relies on the formation of hydroxide groups on the oxide surface after chemisorption of water molecules (13). These groups interact with protons in solution through the Grotthuss mechanism (proton hopping), as illustrated in Figure 1.

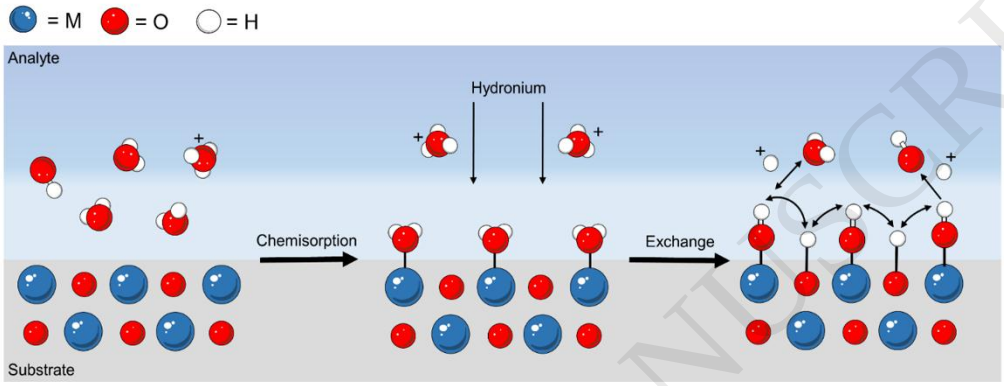


FIGURE 1: Illustration of the pH sensing mechanism of metal oxides. When immersed in an analyte, water is chemisorbed onto the surface. The formed groups are able to interact with the protons in solution (hydronium) through proton hopping between the hydroxylated sites. As a result the surface potential changes with respect to pH.

The reactions governing the pH sensitive properties for $IrO_x$ and $RuO_x$ are.

$$IrO_x: \quad 2IrO_2 + 2H^+ + 2e^- \rightleftarrows Ir_2O_3 + H_2O \qquad (Eq.1)$$

$$RuO_x: \quad 2RuO_2 + 2H^+ + 2e^- \rightleftarrows Ru_2O_3 + H_2O \qquad (Eq.2)$$

In practice, these reactions involve oxyhydroxides within the film, which result in their distinct pH sensitive properties. Combining these equations with the Nernst-equation gives a simplified term for the electrode potential *E*:

$$E = E^{0\prime} - 2.303\frac{RT}{zF}pH \qquad (Eq.3)$$

Here, *R* is the universal gas constant, *T* the absolute temperature, *z* the number of electrons, and *F* Faraday's constant. If $z = 1$ and $T = 298$ K, a theoretical Nernstian sensitivity of -59 mV $pH^{-1}$ is obtained. As described by *Hitchman and Ramanathan* (13), the formal potential ($E^{0\prime}$) of pH sensitive metal oxides is highly dependent on the amount of redox couple present within the film and its degree of hydration (8, 21, 22). For $IrO_x$, the stability of $E^{0\prime}$ is determined by the ratio of the Ir(III) and Ir(IV)

oxidation state. The latter has an increased proton exchange capacity facilitated by the $OH^-$ groups on the surface (13, 22). Over time a reduction in these sites leads to a change in $E^{0\prime}$. It is this change in formal potential that makes recalibration inevitable. In contrast, the sensitivity remains stable (7, 13, 23, 24). It is clear from equation 1 and 2 that changes in the ratios between the redox couple results in a change in the calibration curve. Drift correction is thus performed from the change in the formal potential, obtained by linear regression. Low drift rates below 1 mV $hour^{-1}$ have been reported for Iridium oxides. However, in many cases, the measured time scale rarely exceeds a month. Although $RuO_x$ is governed by the same ratiometric and ageing effects, to our knowledge it is still unclear how it performs.

A second aspect of the performance of a MO pH sensor is surface roughness. The roughness can increase the number of sites contributing to pH sensitivity and affects stability due to the quantity of oxyhydroxides across the film (7, 13, 22). Increasing the roughness increases the effective surface area, thus increasing the capacitance of the electrical double layer; important for electrical impedance sensors. These effects were measured using surface profiling (AFM) and electrochemical impedance spectroscopy (EIS). The performance of the pH sensitive MO films was characterised based on the Nernst-equation i.e. $E^{0\prime}$ and the sensitivity, as well as the surface roughness and electrode impedance.

## Materials and methods

**Sensor chips.** Platinum (Pt) electrodes were fabricated by standard photolithography and etching. 200 nm of Pt (99.99% Testbourne Ltd, UK) was deposited onto borosilicate substrates with a 20 nm Titanium (Ti) (99.99% Testbourne Ltd, UK) adhesion layer (Orion Sputter, AJA, USA). Electrodes were patterned using ion-milling (Ionfab 300, Oxford Instruments, UK). A passivation layer was deposited across the tracks. The bare Pt sensor chips were used as a control and also as a substrate for deposition of $IrO_x$ films. A cross-sectional view and a picture of the sensor chip is shown in Supl.1.

**Electrochemical Iridium Oxide Film (EIROF).** Electrochemical deposition was performed using a 3-electrode cell consisting of a Pt electrode (the sensor), a Pt counter electrode, and a commercial Silver/Silver-chloride (Ag/AgCl) reference electrode with 3M internal filling (Single Junction, Sigma Aldrich, UK). An adhesion layer of Gold (Au) was first plated onto the platinum electrode using electrodeposition at constant current (1 mA $cm^{-2}$) with a gold plating solution (Spa Plating Ltd., UK) and a PalmSense3 potentiostat (PalmSense b.v., The Netherlands). The Au plated electrodes were rinsed in DI water and immediately used for EIROF formation.

EIROF deposition followed the method of *Yamanaka* (25). Stock solutions were prepared as follows: 0.5 g of $IrCl_4$ hydrate (Sigma Aldrich, UK) was dissolved in 100 mL of deionised (DI) water and

stirred for 30 minutes. Next, 10 mL of 30% v/v hydrogen peroxide (Sigma Aldrich, UK) was added and left to stir for 10 min. After, 0.5 g of oxalic acid dehydrate (Sigma Aldrich, UK) was added and stirred for 10 minutes. Potassium carbonate (Sigma Aldrich, UK) was added gradually until a pH of 10.5 was achieved. The solution was left to stir overnight before aliquoting for further use. Aliquots were stored at 4 $^0$C and allowed to reach room temperature before use. EIROF electrodeposition was performed using cyclic voltammetry with potential sweeps between +0.2 V and +0.7 V for a minimum of 125 cycles at a 50 mV $s^{-1}$ scan rate, after which a blue EIROF film formed.

**Ruthenium Oxide Film (RUOF).** Ruthenium oxide sensors were made by sputtering from a $RuO_x$ target (99.8% purity, Testbourne Ltd, UK)) onto Pt electrodes. The $RuO_x$ film was patterned by lift-off. A 250 nm film of $RuO_x$ was deposited onto the Pt electrodes at 75 W in a 80:20 Ar:$O_2$ ratio at 3 mTorr chamber pressure (26). Prior to $RuO_x$ deposition a thin seed layer of Au or Ti (5 nm) was deposited. Between deposition of the seed layer and $RuO_x$, the chamber was kept under vacuum. A post annealing step at 420 $^0$C (80:20, $N_2$:$O_2$), was performed on some sensors to change the morphology of the $RuO_x$ film, and improve adhesion to the underlying layer (27). These annealed films were imaged using Atomic Force Microscopy (Multimode Nanoscope V, Veeco). An image of the RUOF3A sensor chip is shown in Supl.2.

**Encapsulation of sensors.** Wires were soldered to Pt pads and the sensor encapsulated in epoxy (RS Components, UK) in two stages. The first stage encapsulated the solder joint and fixed the wires in place. Next, the sensor chip was pushed through a small pipette tip which was back-filled with epoxy. This process produced sensors with no measurable water absorption in the epoxy. Occasional water ingress was seen as a rapid drop in potential and confirmed by short-circuit measurement across the terminals. Recording was terminated when this was seen.

**Experimental details.** Initially the sensors were immersed in phosphate buffered saline (PBS) at elevated temperature (100 $^o$C or 37 $^o$C for 3 to 12 hours respectively) and then imaged. All potentiometric measurements were performed with a temperature bath (SWB-20L-2, Cleaver Scientific Ltd., UK) set to 37.5 ± 2 $^0$C, unless specified otherwise. For pH calibrations, commercial buffer solutions (pH 4, 6, 7, 9 and 10) were used (Hannah Instruments, UK). A commercial glass pH probe measured the pH immediately after sensor measurements were taken. Buffers were allowed to equilibrate by placing them in the temperature bath prior to pH recordings. The commercial pH probe was calibrated under the same conditions. A commercial double junction Ag/AgCl RE with 3M KCl internal filling (Sigma Aldrich, UK) was used for the reference potential. The electrode potential stability was checked prior to the experiments against a master reference electrode from the open circuit potential (OCP). For long-term measurements, sensors were immersed in PBS. This solution evaporated with time but was replenished as needed with DI water. The pH of the solution was checked prior to calibration, and on a weekly basis.

The OCP of EIROF and RUOF sensors was measured with a high input impedance port (pH/ORP adapters (Robot Shop, UK) running in pH mode with a minimum resolution of 1 mV and NI DAQ USB6211 (National Instruments, USA)). Data were recorded initially every second, and then at 30 min intervals. Data was processed using an 1800 points average filter (30 minute period) to reduce noise.

Calibration was performed for a minimum of 30 minutes in each buffer solution. The final, stable part of the graph (between 500-1000 data points), was used to compute the average and standard deviation of a linear regression fit (in Origin 9.1). The impedance of the sensors was measured with a PalmSense3 potentiostat with a 100 $mV_{p-p}$ excitation signal; 1 Hz – 50 kHz. For the measurements, sensor chips with two electrodes were used (area = 0.092 $cm^2$; electrode separation = 2 mm).

**Results and discussion**

**MO adhesion.** It has been reported that delamination of both EIROF and thermally formed $IrO_x$ films can be overcome by adding a protective coating such as Nafion® or polyethylenimine to the sensor surface, with the added benefit of limiting biofouling (7, 10, 28, 29). Although this might be a necessity in certain applications such as *in vivo* sensing, this can significantly increase the response time (10). In this work, adhesion of the MO films was measured on Au and Pt/Ti electrodes. Accelerated failure was performed by boiling the deposited films in DI water and PBS for 3-12 hours. Delamination and cracking of the film was observed, leading to shattering and peeling, leaving the underlying metal exposed. Images of RUOF3 and EIROF samples are available in in Supl.3; the adhesion results are summarised in Table 1. The data shows that a Ti seed layer improved the adhesion of the deposited $RuO_x$ films. With no delamination for the annealed $RuO_x$ irrespective of the seed layer used. This could be due to alloying of the metals improving adhesion. It has been shown that annealing reduces stress in RF magnetron sputter deposited thin films (30). In contrast, EIROF delaminated on both Au and Pt surfaces. For further assessment, two types of $RuO_x$ sensors were made: one with a Ti seed layer with annealing (referred to as RUOF3A); and a second without annealing and no Ti (referred to as RUOF3). As reported in the literature, Au has good adhesion to $IrO_x$ with good long-term stability (12, 16, 23, 24). Therefore, for comparison, a third sensor (EIROF with Au layer) was fabricated for further characterisations.

Table 1. Summary of experimental data for EIROF and RUOF sensors.

| **Type** | **Substrate** | **Delam. (100 $^0$C)** | **Delam. (37 $^0$C)** | **Sensitivity (mV $pH^{-1}$)** | ***E$^0$'*** **(mV)** | **Conf. interval (99.7%)** |
|---|---|---|---|---|---|---|

| | | | | | | |
|---|---|---|---|---|---|---|
| EIROF | Platinum | Yes | Yes | -72.2 ± 1.9 | 893.3 ± 22.0 | ±0.08 pH |
| EIROF | Gold | Yes | No | -72.5 ± 1.1 | 775.9 ± 21.0 | ±0.05 pH |
| RUOF3 | Platinum | Yes | NA | -56.2 ± 3.8 | 595.8 ± 17.3 | ±0.20 pH |
| RUOF3A | Titanium | No | No | -59.3 ± 4.7 | 609.3 ± 21.2 | ±0.24 pH |

**Electrochemical characteristics.** Cyclic voltammograms (CV) for both EIROF and RUOF are shown in Figure 2a-b. Peaks associated with the oxidation states of the MOs can clearly be observed. For EIROF, these are located at +0.7 V versus Ag/AgCl (3M KCl), in agreement with other work (13, 22). The electrochemical characteristics for RUOF on Ti are shown in Figure 2b (note films on Pt delaminated when the potential was swept). Multiple peaks were observed for RUOF on Ti as reported by *Chalupczok et al* (21). The pH sensitivity is dominated by the Ru(III) and Ru(IV) redox couple (Eq. 2)), located beyond +250 mV versus Ag/AgCl 3M (in PBS pH 7.45) as shown in Figure 2b. The peak separation $\Delta Ep$ between the cathodic and anodic peaks, yields an electron transfer number $z \approx 1.2 \pm 0.4$ averaged across the scan rates. This variation could be due to increased roughness of the film, as observed for EIROF (31), but could also be due to the small changes in pH local to the surface generated during the sweep.

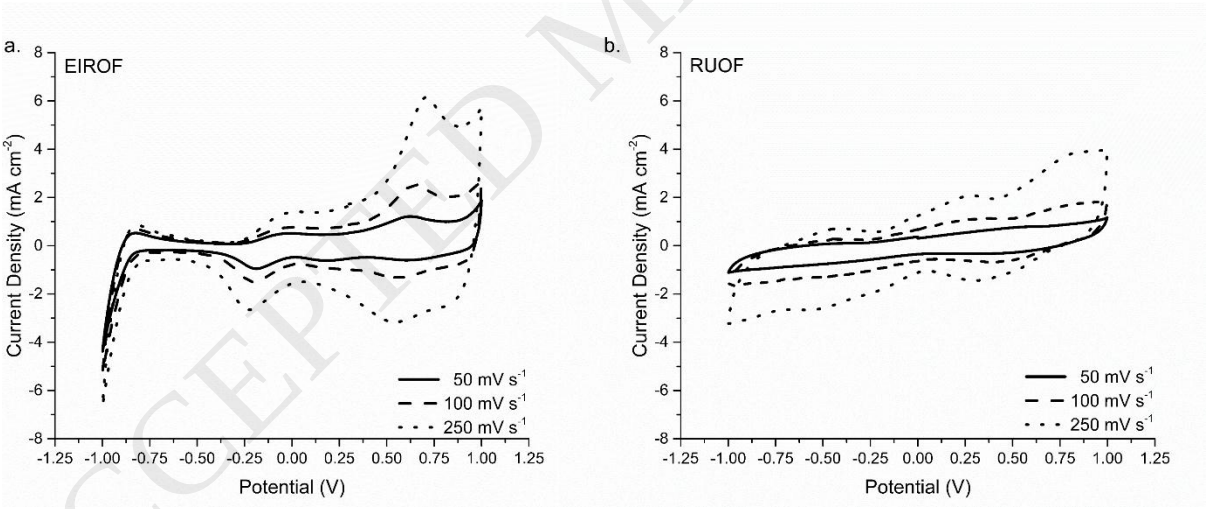

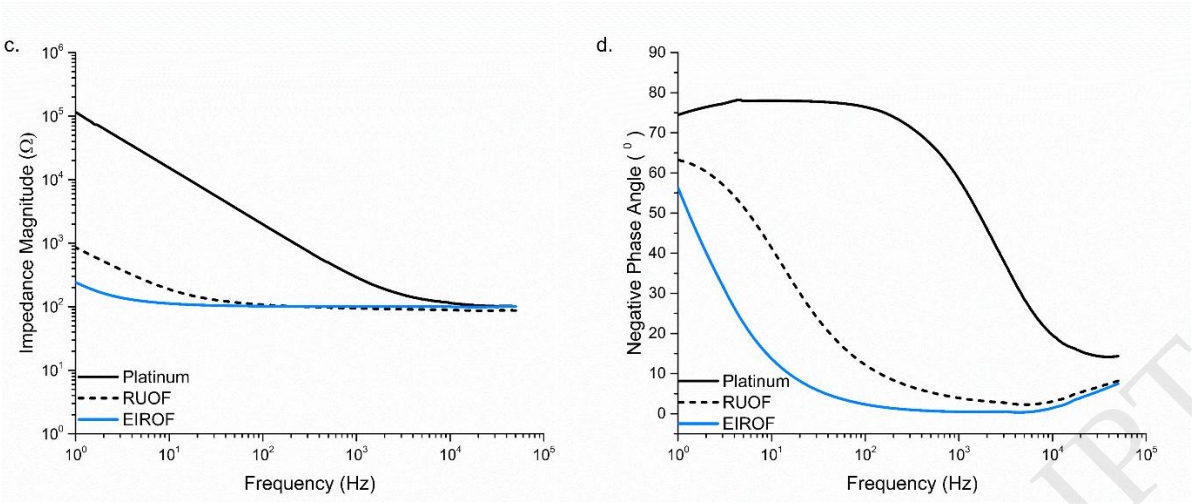


FIGURE 2: Cyclic voltammograms for a) EIROF and b) RUOF in PBS at room temperature for different scan rates. The peaks for the RUOF are located at +272 and +322 mV, +337 and +402 mV, +570 and +475 mV versus Ag/AgCl (3M), respectively for decreasing scan rate. The current is normalised to the geometric area of the electrodes. c) Impedance magnitude and d) phase angle for Platinum, RUOF and EIROF in PBS with conductivity 1.4 S $m^{-1}$ across a frequency range from 1Hz – 50 kHz with 100 $mV_{p-p}$ AC signal.

**Impedance characterisation**. The electrical impedance of EIROF and RUOF surfaces were measured and compared with sputter deposited bright Platinum; the magnitude and phase angle data are shown in Figure 2c-d. Fitting the data to the Randles equivalent circuit model using a Constant Phase Element for the Electrical Double layer, give the interface capacitance of 4.9, 162.0 and 752.0 μF $cm^{-2}$ for Pt, RUOF and EIROF respectively. These values are similar to the trends reported for sputtered Iridium Oxide and Platinum black (32), confirming the large effective surface area for the RuOx thin films. The RUOF3A has a rougher surface because the annealing step forms larger grain structures by filling vacancies in the lattice. Using AFM, the roughness of the RUOF3 and RUOF3A was measured to be 5.6 ± 3.2 nm rms and 11.8 ± 2.4 nm rms respectively - see Figure 3.

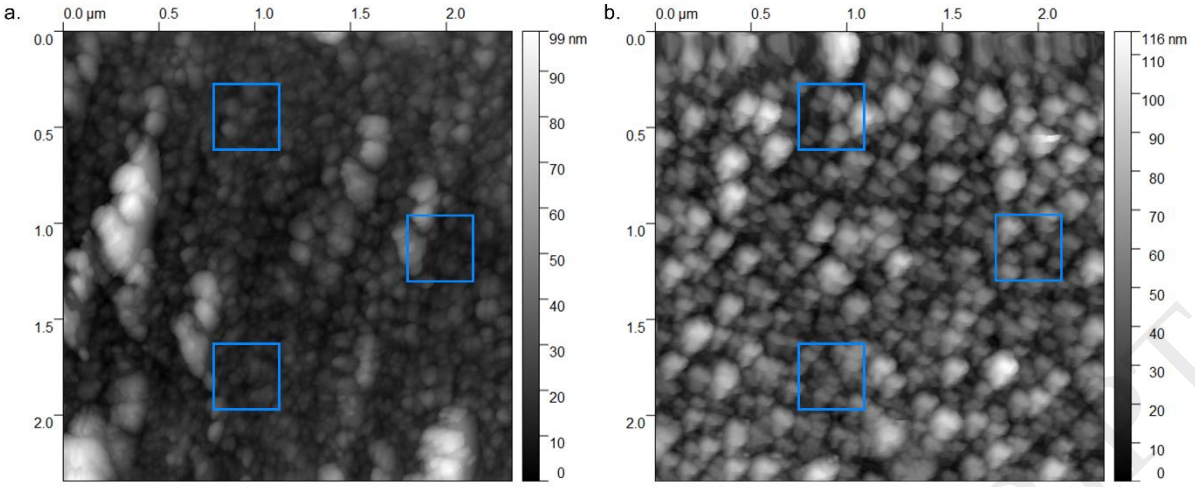


FIGURE 3. Atomic Force Microscopy images of a) RUOF3 and b) RUOF3A samples. Blue boxes were used to compute the roughness, which was 5.6 ± 3.2 nm rms and 11.8 ± 2.4 nm rms for a) and b), respectively.

**pH performance: short-term.** The sensitivity of freshly deposited EIROF and RUOF sensors was assessed using a linear regression fit to the potential vs. pH plots; example calibration curves are shown in Figure 4a-b. Data for Pt is shown for reference, with a measured sensitivity of -42 mV $pH^{-1}$. As a Pt substrate is used, this value serves as a control to detect sensor failure caused by delamination or exposed Pt. Super-Nernstian responses were observed for EIROF samples, with an average sensitivity and standard error of -72.5 ± 1.1 mV $pH^{-1}$, see Table 1. The EIROF surfaces were characterised by a 99.7% confidence interval (based on three times the standard error) of ±0.05 pH, close to the accuracy of the commercial glass pH probe. The measured value is in good agreement with the values found in literature. (23, 24, 33, 34) . The sensitivity of the RuOx films were measured at -56.3 ± 0.2 mV $pH^{-1}$ for RUOF3 and -55.0 ± 0.3 mV $pH^{-1}$ for RUOF3A, similar to the reported values of -55 to -60 mV $pH^{-1}$ (17-19, 26). For the RUOF3A samples (with increased roughness) little difference between freshly made RUOF3 and RUOF3A was observed. After immersing the metal oxides for 7 days in PBS the sensitivity of the RUOF3A increased slightly by -2.9 mV $pH^{-1}$, most likely due to hydration of the film. The average values for sensitivity and $E^{0\prime}$ with the standard errors of the linear regressions are listed in Table 1. As can be denoted, there is no significant difference between the sensitivities found for the RUOF3 and RUOF3A.

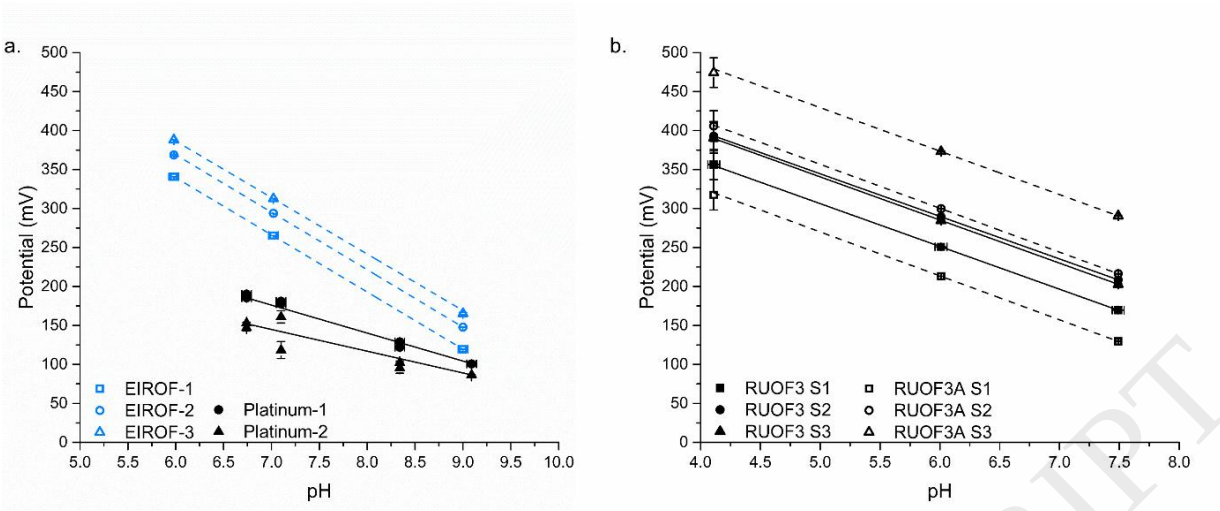


FIGURE 4. Example Calibration curves for a) EIROF and platinum and b) RUOF3 and RUOF3A. Lines are linear regression with $R^2 > 0.999$ for EIROF, RUOF3 and RUOF3A samples. Average sensitivities equal -72.1 ± 1.1 mV $pH^{-1}$, -56.3 ± 0.2 mV $pH^{-1}$ and -55.0 ± 0.3 mV $pH^{-1}$, respectively.

The short-term precision of $IrO_x$ films has been reported on extensively (23, 24, 33, 34). However the short-term characteristics of RUOF sensors are unknown. Accuracy was measured by titration against a glass pH probe using additions of $H_2SO_4$. The results are shown in Figure 5a, and a summary of the short term precision for the $RuO_x$ films is shown in Figure 5b. The pH difference (ΔpH) represents the absolute error between the sensor reading converted to a pH value, and the commercial probe. The precision represents the percentage of all readings acquired from all sensors tested (Figure 5a) that fall within a given ΔpH band. This data shows that RUOF3 has the best performance, compared with the annealed samples that have a lower precision.

The superior performance of RUOF3 could be due to the lower deposition pressure that might lead to a denser film. Both annealing temperature and deposition pressure affects the morphology of the film (27). The surface of the $RuO_x$ might stabilise more quickly compared to the rougher structure of the annealed films as the increased density of oxyhydroxide sites contribute to the potential stability over time (13, 22).

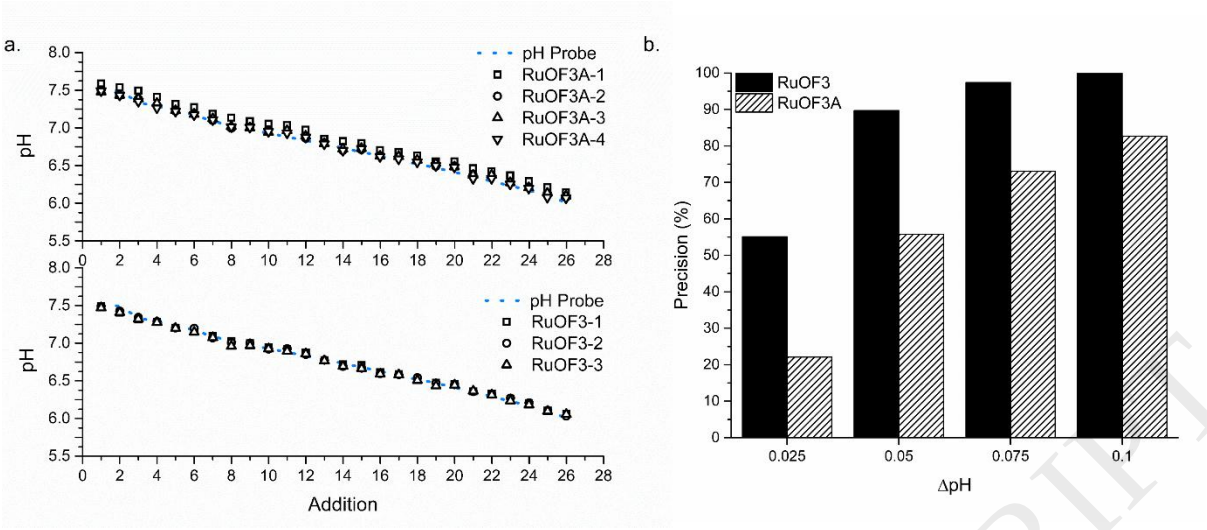


FIGURE 5: a) Titration curves for RUOF3A and RUOF3 versus a Hannah Instruments glass pH probe. Titrated in PBS using 0.1M $H_2SO_4$. b) Precision as a percentage within a set ΔpH band for RUOF3 and RUOF3A, with 78 and 104 measurement points, respectively.

**pH performance: Long-term.** Sensitivity and formal potential measurements of the metal oxide sensors, measured over 40 days, are presented in Figure 6. The EIROFs have a higher formal potential and sensitivity compared to RUOFs; the drift in $E^{0}$' is -0.85 to -2.0 mV day$^{-1}$ and the drift in sensitivity is 0.5 ± 0.2 mV week$^{-1}$ ($R^2$ = 0.89), confirming that the formal potential is the main contributor to drift for EIROF sensors (sensitivity remains stable). In contrast, the formal potential for RUOF was varying implying that no drift characteristics can be distinguished.

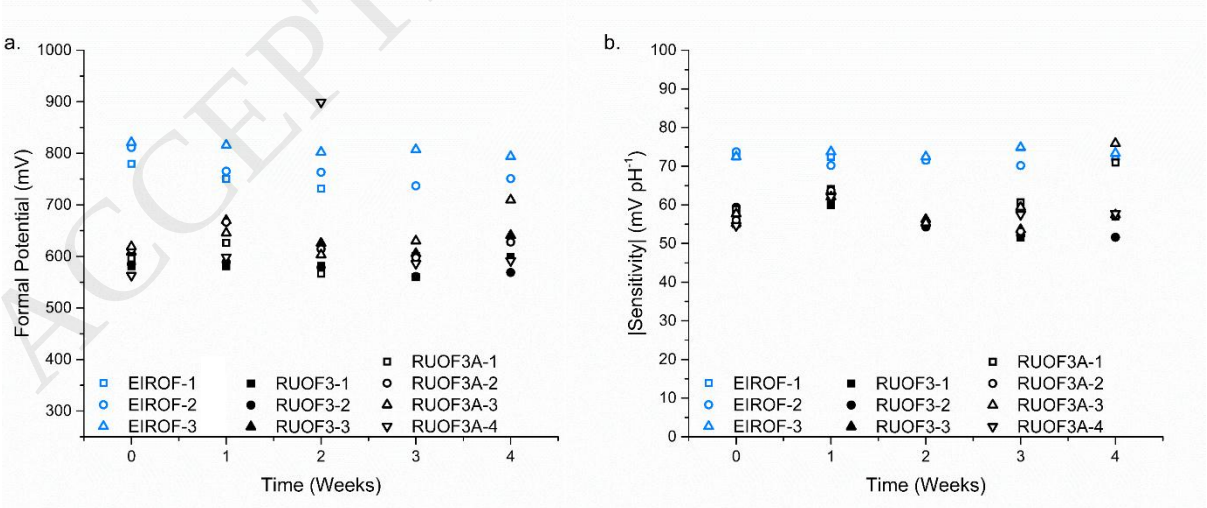

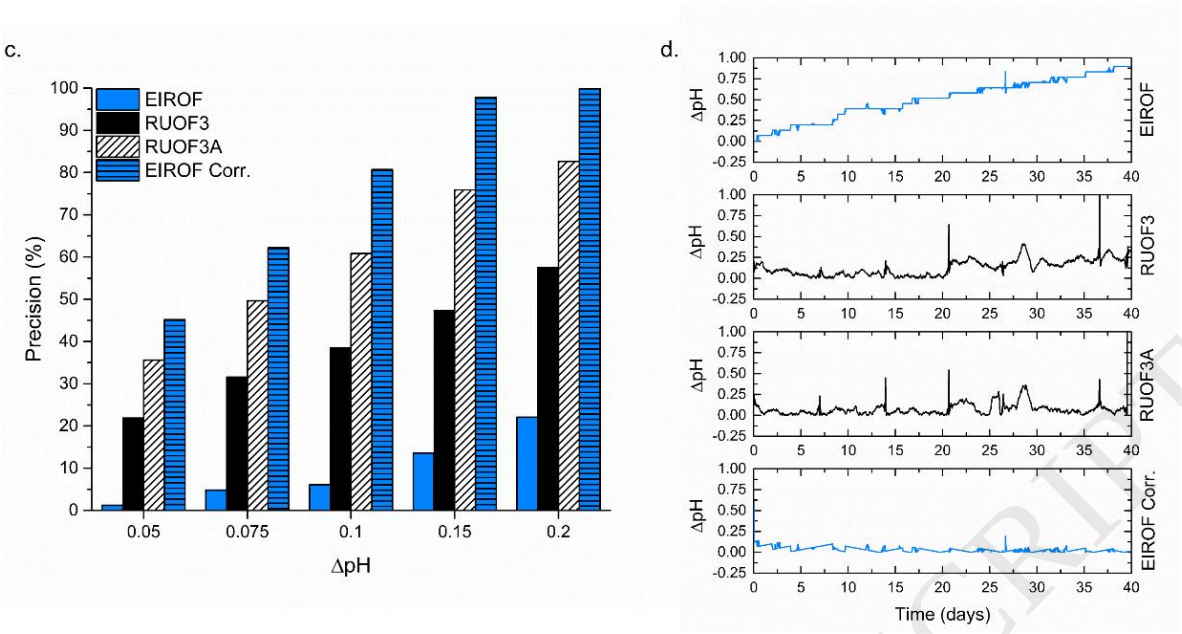


FIGURE 6. Weekly assessment of a) formal potential and b) sensitivity over a 40 day period (PBS at 37.5 ± 2 $^{0}$C). c) Precision as a percentage within a set ΔpH for all samples in the set. Values based on data points taken at 30 minute intervals over the measurement period with a total number of 4694, 6108, 6584 measurement points for EIROF, RUOF3 and RUOF3A, respectively. d) Example traces for ΔpH for EIROF and RUOF, and EIROF corrected for drift. Spikes in data are the weekly calibration points. Note: data for EIROF-1 is only shown up to week 2 due to failure of the encapsulant.

In contrast to the constant drift in EIROF, the variability in $E^{0\prime}$ for RUOF indicates that a re-calibration would be required depending on the specified confidence interval. To determine the long term-behaviour of the metal oxides, the pH value for each sensor was measured (potential versus Ag/AgCl) determined using the calibration curve and compared with a Hannah instruments glass pH probe. The RUOFs were hydrated for 1 week prior to measurement and calibration. This difference (ΔpH) was determined and plotted in as a percentage and trace in Figure 6 c-d.

The long-term accuracy of EIROF is governed by the drift in $E^{0\prime}$, and from the data this metal oxide exceeds the ±0.1 ΔpH band within 3 days (Fig 6d). However, because the drift is linear the error can be corrected by using the fit to the formal potential. This keeps the value of ΔpH for the EIROFs within a ±0.15 pH band over 40 days; see EIROF Corr. bar and trace in Figure 6c-d. Note that compensating for drift with EIROF sensors is an advantage over RUOF in applications where the drift is known and remains constant. For RUOF3, the precision values do not exceed 57.6% for a ΔpH of ±0.2 pH. Examining the error plot in Figure 6d shows that the error remains within its confidence interval of ±0.2 pH until day 20. For RUOF3A the precision values are 82.7% for the same ΔpH. The outliers, such as those observed from day 25-26, are the main reasons why the precision is not as high as predicted by the confidence interval; the cause of these is currently unknown.

To assess the long term behaviour RUOF3A the sensors were immersed in buffer for a total of 21 weeks and sensitivity and formal potential recorded at weeks 0-4 (Fig 6), and resumed from weeks 18 to 21 (Figure 7). Figure 7 shows that the trend in the formal potential is similar to that observed in Figure 6a. The average value of $E^{0\prime}$ over this 4 week period (weeks 18-21) was 644 ± 29 mV $pH^{-1}$; an increase of 34 mV from the mean over weeks 0-4 (Table 1), equal to a shift of 0.56 pH over this time interval. The sensitivity remained unchanged with an average of -58.5 ± 3 mV $pH^{-1}$. These results indicate that for RUOF3A sensors, the drift in $E^{0\prime}$ dominates, whilst the sensitivities remain constant. Prolonged immersion in buffer does not appear to adversely affect the metal oxides or compromise the performance significantly.

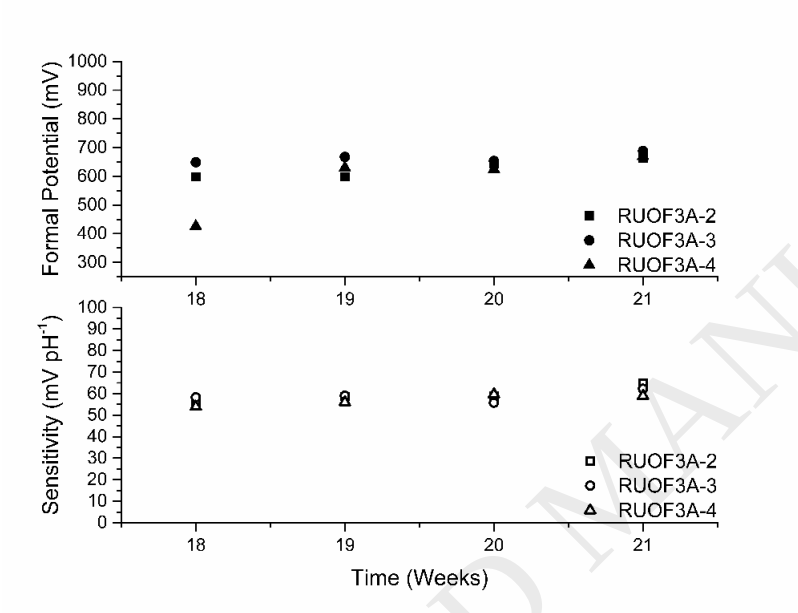


FIGURE 7. Long-term performance of RUOF3A sensors immersed in PBS at 37.5 ± 2 $^0$C, measured from weeks 18 to 21. Data from three sensors are shown; sensor "RUOF3A-1" failed due to water ingress into the encapsulant.

Overall, the data show that the $IrO_x$ sensor gives superior performance compared with $RuO_x$ only if the long-term drift can be quantified and the data corrected. Practically this means that the sensor has to be periodically re-calibrated to determine the drift in $E^{0\prime}$, with a required recalibration post measurement. In contrast the $RuO_x$ sensors, particularly the annealed film, has a stable $E^{0\prime}$, within a given band which means that sensors made from this metal oxide can be used without intermittent calibration.

**Conclusion**

The pH sensing properties of metal oxide sensors made of Ruthenium (un-annealed and annealed) and Iridium have been analysed and compared. Short-term characteristics indicated excellent performance for both types with near-Nernstian sensitivities for RUOFs compared to super-Nernstian responses for

EIROFs. The large surface area of the metal oxide films leads to a significantly increased double layer capacitance at low frequencies - the rougher nature of the electrodes was also confirmed by AFM. EIROF films have excellent short-term characteristics, but their long-term performance means that regular recalibration for drift correction is required. Long-term performance measurement show that annealed $RuO_x$ films have the highest precision for a given ΔpH of ±0.2 pH over 40 days. However, the variation in formal potential during prolonged periods (21 weeks) means that recalibration of RUOF sensors would be needed depending on the acceptable error. The accuracy of both RUOF3 and RUOF3A sensors is superior to the $IrO_x$ sensors, which given the much lower cost of this metal makes them suitable for low-cost applications such as *in vivo* sensors or remote environmental and maritime applications where continuous re-calibration cannot be performed or is undesirable.

**Acknowledgements**

This study/project is funded by the National Institute for Health Research (NIHR) (i4i programme project reference II-LB-0715-20002). The views expressed are those of the author(s) and not necessarily those of the NIHR or the Department of Health and Social Care. The authors thank Vivoplex Medical Ltd. and in particular Dr. S. Lu for his advice on the project.

**Conflict of interest**

The authors declare no conflict of interest.

**References**


1. Marczewska B, Marczewski K. First Glass Electrode and its Creators F. Haber and Z. Klemensiewicz – On 100th Anniversary. Zeitschrift für Physikalische Chemie2010. p. 795.
2. Myers RJ. One-Hundred Years of pH. Journal of Chemical Education. 2010;87(1):30-2.
3. Bergveld P. Development of an Ion-Sensitive Solid-State Device for Neurophysiological Measurements. Biomedical Engineering, IEEE Transactions on. 1970;BME-17(1):70-1.
4. Vonau W, Guth U. pH Monitoring: a review. Journal of Solid State Electrochemistry. 2006;10(9):746-52.
5. Bergveld P. Thirty years of ISFETOLOGY: What happened in the past 30 years and what may happen in the next 30 years. Sensors and Actuators B: Chemical. 2003;88(1):1-20.
6. Marzouk SAM, Ufer S, Buck RP, Johnson TA, Dunlap LA, Cascio WE. Electrodeposited Iridium Oxide pH Electrode for Measurement of Extracellular Myocardial Acidosis during Acute Ischemia. Analytical chemistry. 1998;70(23):5054-61.
7. Ng SR, O'Hare D. An iridium oxide microelectrode for monitoring acute local pH changes of endothelial cells. Analyst. 2015;140(12):4224-31.
8. Kurzweil P. Metal Oxides and Ion-Exchanging Surfaces as pH Sensors in Liquids: State-of-the-Art and Outlook. Sensors. 2009;9(6):4955-85.
9. Jasiński D, Meredith J, Kirwan K. The life cycle impact for platinum group metals and lithium to 2070 via surplus cost potential. The International Journal of Life Cycle Assessment. 2018;23(4):773-86.
10. Marzouk SAM. Improved Electrodeposited Iridium Oxide pH Sensor Fabricated on Etched Titanium Substrates. Analytical Chemistry. 2003;75(6):1258-66.
11. Bezbaruah AN, Zhang TC. Fabrication of Anodically Electrodeposited Iridium Oxide Film pH Microelectrodes for Microenvironmental Studies. Analytical Chemistry. 2002;74(22):5726-33.
12. Huang W-D, Cao H, Deb S, Chiao M, Chiao JC. A flexible pH sensor based on the iridium oxide sensing film. Sensors and Actuators A: Physical. 2011;169(1):1-11.
13. Hitchman ML, Ramanathan S. Considerations of the pH dependence of hydrous oxide films formed on iridium by voltammetric cycling. Electroanalysis. 1992;4(3):291-7.
14. Huang X-r, Ren Q-q, Yuan X-j, Wen W, Chen W, Zhan D-p. Iridium oxide based coaxial pH ultramicroelectrode. Electrochemistry Communications. 2014;40:35-7.
15. Wang M, Yao S, Madou M. A long-term stable iridium oxide pH electrode. Sensors and Actuators B: Chemical. 2002;81(2–3):313-5.
16. Nguyen CM, Rao S, Yang X, Dubey S, Mays J, Cao H, et al. Sol-gel deposition of iridium oxide for biomedical micro-devices. Sensors. 2015;15(2):4212-28.

17. Tanumihardja E, Olthuis W, Van den Berg A. Ruthenium Oxide Nanorods as Potentiometric pH Sensor for Organs-On-Chip Purposes. Sensors. 2018;18(9).
18. Tanumihardja E, Olthuis W, Berg Avd. Ruthenium Oxide pH Sensing for Organs-On-Chip Studies. Proceedings. 2018;2(13).
19. Lonsdale W, Wajrak M, Alameh K. Manufacture and application of RuO2 solid-state metal-oxide pH sensor to common beverages. Talanta. 2018;180:277-81.
20. Brischwein M, Grothe H, Wiest J, Zottmann M, Ressler J, Wolf B. Planar Ruthenium Oxide Sensors for Cell-on-a-Chip Metabolic Studies2009. 1193-201 p.
21. Chalupczok S, Kurzweil P, Hartmann H. Impact of Various Acids and Bases on the Voltammetric Response of Platinum Group Metal Oxides. International Journal of Electrochemistry. 2018;2018:6.
22. Olthuis W, Robben MAM, Bergveld P, Bos M, van der Linden WE. pH sensor properties of electrochemically grown iridium oxide. Sensors and Actuators B: Chemical. 1990;2(4):247-56.
23. Bitziou E, O'Hare D, Patel BA. Simultaneous Detection of pH Changes and Histamine Release from Oxyntic Glands in Isolated Stomach. Analytical chemistry. 2008;80(22):8733-40.
24. Bitziou E, O'Hare D, Patel BA. Spatial changes in acid secretion from isolated stomach tissue using a pH-histamine sensing microarray. Analyst. 2010;135(3):482-7.
25. Yamanaka K. Anodically Electrodeposited Iridium Oxide Films (AEIROF) from Alkaline Solutions for Electrochromic Display Devices. Japanese Journal of Applied Physics. 1989;28(Part 1, No. 4):632-7.
26. Lonsdale W, Wajrak M, Alameh K. RuO2 pH Sensor with Super-Glue-Inspired Reference Electrode. Sensors. 2017;17(9).
27. Kreider KG, Tarlov MJ, Cline JP. Sputtered thin-film pH electrodes of platinum, palladium, ruthenium, and iridium oxides. Sensors and Actuators B: Chemical. 1995;28(3):167-72.
28. Kinlen PJ, Heider JE, Hubbard DE. A solid-state pH sensor based on a Nafion-coated iridium oxide indicator electrode and a polymer-based silver chloride reference electrode. Sensors and Actuators B: Chemical. 1994;22(1):13-25.
29. Trouillon R, Combs Z, Patel BA, O'Hare D. Comparative study of the effect of various electrode membranes on biofouling and electrochemical measurements. Electrochemistry Communications. 2009;11(7):1409-13.
30. Koch R. Stress in Evaporated and Sputtered Thin Films – A Comparison. Surface and Coatings Technology. 2010;204(12):1973-82.
31. Casella IG, Contursi M, Toniolo R. Anodic electrodeposition of iridium oxide particles on glassy carbon surfaces and their electrochemical/SEM/XPS characterization. Journal of Electroanalytical Chemistry. 2015;736:147-52.

32. Malleo D, Nevill JT, van Ooyen A, Schnakenberg U, Lee LP, Morgan H. Note: Characterization of electrode materials for dielectric spectroscopy. Review of Scientific Instruments. 2010;81(1):016104.
33. Chu J, Zhao Y, Li S-H, Yu H-Q, Liu G, Tian Y-C. An Integrated Solid-State pH Microelectrode Prepared Using Microfabrication. Electrochimica Acta. 2015;152:6-12.
34. Carroll S, Baldwin RP. Self-Calibrating Microfabricated Iridium Oxide pH Electrode Array for Remote Monitoring. Analytical chemistry. 2010;82(3):878-85.

**Dr. Roeland H.G. Mingels**

Roeland Mingels is a Post-Doctoral Researcher at the Biomedical Electronics research group, part of the School of Electronics and Computer Science at the University of Southampton. He has completed his Ph.D in sensor development with a particular interest in long-term sensing applications for both environmental and biomedical research. Throughout his Ph.D and Post-Doctoral research he has collaborated with industry to commercialise the research outcomes and has filed several patents in the process. He is currently working on the development of an implantable sensor platform in collaboration with Vivoplex Medical Ltd.

**Dr. S.Kalsi**

Sumit Kalsi completed his PhD at the University of Southampton in 2013 on a project aimed at development of miniaturised technologies for intramembrane protein characterisation. Since the completion of his PhD, he has worked on several projects in collaboration with industry towards the development of in-vitro diagnostic and drug discovery platforms, having microfluidics as recurring theme for fluid handling. Currently, he is working as a research fellow with Prof. Hywel Morgan and Prof. Ying Cheong on the development of an implantable electrochemical sensor platform in collaboration with Vivoplex Medical Ltd.

**Prof. Y. Cheong**

Ying Cheong is the Professor of Reproductive Medicine in the University of Southampton. Her interest is in cross discipline research on technologies which can improve reproductive outcomes. She is an experienced clinical trialist, leads the Clinical research network for Hampshire and Isle of Wight, the national lead for commercial portfolio studies, and is the PI of several NIHR and MRC funded portfolio studies.

**Prof. H.Morgan**

Hywel Morgan is Professor of Bioelectronics and deputy director of the University of Southampton Institute for Life Sciences. He is also deputy Head of the School of Electronics and Computer Science and leads the Biomedical Electronics research group. He has published over 250 peer reviewed papers (H-index 60) and co-authored a text-book on AC electrokinetics. He has 12 granted patents and has licenced technology to several companies. In 2012 he was awarded a Royal Society Industry Fellowship with Sharp Labs and co-founded a spin-out to commercialise in vivo wireless sensors. He is currently associate editor for Microfluidics and Nanofluidics. He holds a Royal Society Wolfson research merit award.